Facile Preparation and Electrochemical Investigations of Copper-Ion Doped α-MnO_2 Nanoparticles

Nigus Gabbiye Habtu[1,3(✉)], Ababay Ketema Worku[1], Delele Worku Ayele[1,2(✉)], Minbale Admas Teshager[4], and Zerihun Getahun Workineh[5]

[1] Bahir Dar Energy Center, Bahir Dar Institute of Technology, Bahir Dar University, P.O. BOX 26, Bahir Dar, Ethiopia
{nigus.gabiye, Delele.worku}@bdu.edu.et
[2] Department of Chemistry, Bahir Dar University, P.O. Box 79, Bahir Dar, Ethiopia
[3] Department of Chemical Engineering, Bahir Dar Institute of Technology, Bahir Dar University, P.O. Box 26, Bahir Dar, Ethiopia
[4] Department of Chemistry, Debre Markos University, P.O. Box 269, Debre Markos, Ethiopia
[5] Department of Materials Science and Engineering, Bahir Dar University, P.O. BOX 79, Bahir Dar, Ethiopia

Abstract. Copper doped MnO_2 nanoparticles have been developed by co-perception technique without using any surfactants and templates. The physiochemical and thermal properties of the as-prepared nanoparticles have been analysed by X-ray diffraction (XRD), Fourier transform infrared (FTIR) spectroscopy, and Thermogravimetric analysis (TGA) and/or Differential thermal analysis (DTA). The catalytic performance of MnO_2 and Cu doped MnO_2 nanoparticles have been assessed via cyclic voltammetry (CV). The crystal structure of MnO_2 and Cu doped MnO_2 nanoparticles was the sharply crystallized α-MnO_2. However, the Copper dopant has no noticeable influence on the crystallization of MnO_2 as determined by the results of XRD analysis. The formation of M-O (M = Mn, Cu) was confirmed from FTIR study. Cu-doped MnO_2 nanoparticles showed improved thermal stability as confirmed by TGA/DTA analysis. The doping amount had a high impact on the catalytic performance of the Cu-MnO_2 nanoparticles. The Cu-MnO_2 nanoparticles showed better catalytic performance as compared to pure MnO_2. Hence, Cu-doped MnO_2 nanoparticles showed improved catalytic activity and thermal stability.

Keywords: Copper-ion · α-MnO_2 nanoparticles · Co-perception technique · Oxygen reduction reaction

M. L. Berihun (Ed.): ICAST 2021, LNICST 412, pp. 543–553, 2022.
https://doi.org/10.1007/978-3-030-93712-6_36

1 Introduction

Oxygen reduction reaction (ORR) is the principal kinetically restricting the air electrode reaction in energy conversion and storage technologies such as rechargeable metal-air batteries (MABs) and supercapacitors [1, 2]. Preparing electrocatalysts for ORR is a critical issue. Thus, the most extensively used ORR catalysts are yet platinum (Pt) based nanoparticles due to their best performance [3, 4]. However, the practical utilization of Pt for ORR is limited because of its low abundance and high cost [5, 6]. Hence, different kinds of materials such as metal alloys, transition metal oxides, metal oxide, and hybrid materials were mostly used electrocatalysts for ORR [7]. However, utilizing cheap and active oxygen electrocatalysts for ORR remains a big problem [8]. Among these MnO_2 has been used as an electrocatalyst for ORR due to its abundance, novel electrocatalytic performance, low price, and environmentally friendly characteristics. MnO_2 can exist with five types of crystal phases (α-, β-, γ-, δ-, and λ-MnO_2) [9, 10]. The catalytic activity of MnO_2 depends greatly on the crystallographic arrangement, following the order of $\alpha \approx \delta > \gamma > \lambda > \beta$ as stated in the literatures [11, 12]. Investigation on MnO_2 as oxygen electrocatalysts for the ORR associated with the influence of the structure, composition, and morphology, on the catalytic activity [13]. Hence, the most studies have been focused in enhancing the ORR activity via compositing or doping MnO_2 with different transition metals, such as copper (Cu), silver (Ag), iron (Fe), nickel (Ni), and cobalt (Co) doped MnO_2 electrode for ORR application, which change electronic structure and electrochemical performance [14]. To improve these challenges, MnO_2 has been combined with other materials to obtain good electrochemical performance, such as nanocomposites, nanotube @MnO_2, graphene@MnO_2, carbon Co_3O_4@MnO_2, and CuO@MnO_2 [15]. In addition, cation doping has been proven to be an effective method to improve the conductivity of materials. Copper cation is considered to be one of the most suitable candidates for cation doping, as an effective doping cation to enhance the electrochemical performance. However, it is still a challenge to gain high-performance MnO_2 nanomaterials via a low-cost and simple preparation method [16]. Until, similar studies on Cu^{2+} doped MnO_2 nanoparticles for ORR utilization have not been reported very well [17, 18]. Hence, various techniques were applied for the development of doped MnO_2 which includes thermal decomposition, simple reduction [19], solid-phase process, hydrothermal [20], microwave, physical vapour deposition [21], chemical vapour deposition, electro deposition, sol-gel process, aerosol processing, and co-precipitation [22, 23]. Here we have reported the simple co-precipitation technique for the development of different levels of (0.025–0.1M) Cu-ion doped in MnO_2 nanoparticles for ORR application. This study investigates the synthesis of high-performance Cu-ion doped MnO_2 nanoparticles via a low-cost and simple preparation method in an alkaline medium.

2 Materials and Methods

2.1 Chemicals

All chemical were purchased in alpha chemika (India) and utilized without any purifying. Distilled water (DW) was utilized to prepare all solutions. Manganese sulfate monohydrate (99%, $MnSO_4.H_2O$), NaOH solution, potassium permanganate (99.5%, $KMnO_4$), ethanol, and Copper sulfate pentahydrate ($CuSO_4.5H_2O$) were used as precursors.

2.2 Preparation of α-MnO_2 Electrocatalysts

Cu-doped α-MnO_2 and α-MnO_2 nanoparticles were synthesized via co-perception technique. Firstly, 0.3M of $MnSO_4.H_2O$ was dissolved in 40 mL of DW and stirred. Then, $CuSO_4.5H_2O$ desired mole of (0.025, 0.05, 0.075, and 0.1 M) prepared in 40 mL of DW was added dropwise. Additional, 0.2M of potassium permanganate dissolved in 60 mL of DW was added dropwise to the mixture of $MnSO_4.H_2O$ and $CuSO_4.5H_2O$. Adjust the pH of the solution to12 by adding 0.2 M NaOH. After 5 h of stirring at 80 °C the precipitate of Cu doped MnO_2 nanoparticles were obtained. The product was filtered and cleaned with DW. The as-prepared nanoparticles have been dried at 100 °C for 12 h to evaporate water and volatile components. Finally, the as-prepared products were annealed at 500 °C for 3 h. Figure 1 shows schematic illustration of Cu-MnO_2 electrocatalysts preparation via co-precipitation approach.

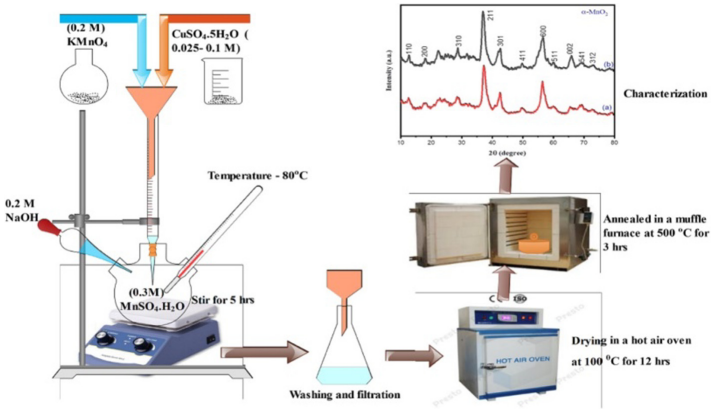

Fig. 1. Schematic illustration of Cu-MnO_2 electrocatalysts preparation by co-precipitation technique.

2.3 Characterization Techniques

The functional groups and other impurities exist in as-prepared samples have been determined via Fourier Transform Infrared spectroscopy (FTIR) (JASCO MODEL FT-IR 6660) in the wavelength range of 400–4000 cm^{-1}. The thermal property was studied

by using TGA/DTA analysis. The XRD patterns of the synthesized nanoparticles were investigated by XRD (SHIMADZU, MAXima_X XRD-7000) with Cu-K_α radiation. Electrochemical analyses were conducted by three electrode CHI760E electrochemical workstation.

2.4 Electrochemical Measurements

A Glassy Carbon Electrode (GCE) of 3 mm has been used as a working electrode. Moreover, the electrode was sonicated with DW and ethanol for 10 min. Ag/AgCl (with an electrolyte of 0.1 M KOH) and Pt coil were utilized as a reference and counter electrodes, respectively. Then, 5 mg of MnO_2 and Cu-doped α-MnO_2 nanoparticles dispersed in a solution of 1 mL (2:1 v/v water/isopropanol mixed) was drop cast (15 mL) constantly on to the GCE electrode surface and dried. Cyclic voltammetry (CV) was conducted at a sweep rate of 50 mV s^{-1} in the range of +0.1 and −0.7 V.

3 Results and Discussion

3.1 Structural Analysis

The structure and phase purity of MnO_2 and Cu-doped MnO_2 nanoparticles were analysed by XRD in a 2θ range of 10–80°. Figure 2 illustrates the XRD pattern of MnO_2 and Cu-doped MnO_2 nanoparticles. As provided in Fig. 2, sharp diffraction peaks had been located at 2θ of 12.67°, 17.99 º, 28.67°, 37.49°, 41.89°, 49.77°, 56.15°, 60.11°, 65.34°, 69.39°, 72.88°, which could be assigned to the (110), (200), (310), (211), (301), (411), (600), (521), (002), (541), and (312) planes of MnO_2 (*JCPDS* 00-*44-0141*). Both XRD peaks shows phase of α-MnO_2 with tetragonal structure. However, with Cu dopant increasing copper oxides or other impurities of XRD peaks were not remarked, showing the high purity of as-prepared α-MnO_2 nanoparticles. The Average crystallite size of the α-MnO_2 and Cu doped MnO_2 were computed through Scherer equation.

$$D = \frac{K\lambda}{\beta \cos\theta} \tag{1}$$

where "K" is the Scherer constant = 0.89, "D" is the crystallites size, "λ" = 1.5406 Å (wavelength of X-rays), "β" (in radians) is the FWHM and "θ" is the peak position. The average crystallite size determined for α-MnO_2 and Cu doped MnO_2 nanoparticles were found to be 4.1 nm and 5.3 nm, respectively. Crystallite size was increased after the doping of copper due to Cu addition into the tunnels.

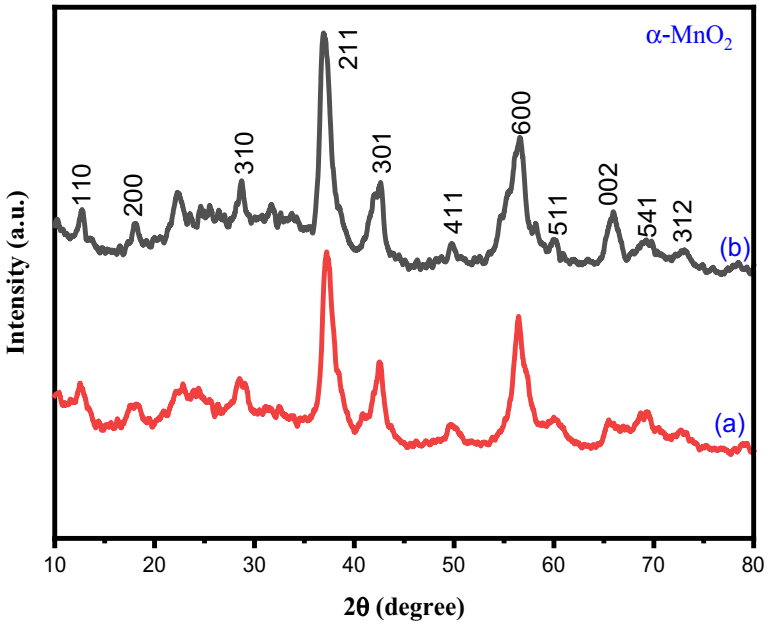

Fig. 2. XRD patterns of (a) MnO_2 and (b) 0.01 M Cu-doped MnO_2 nanoparticles.

3.2 Functional Group Study

FTIR spectra of un-doped MnO_2 and Cu-doped MnO_2 nanoparticles were analysed in the range of 4000–400 cm^{-1}, to investigate the functional groups on the surface of as-prepared materials, and displayed in Fig. 3. The bands located at 3425 cm^{-1} may be because of the stretching vibrations of hydroxyl groups. The peaks at 1647 and 1097 cm^{-1} are corresponding to the bending vibration of structural OH^- and H_2O. The peaks observed at around 521 cm^{-1} are ascribed to the metal-oxygen (M–O) bending vibrations of MnO_2 and Cu doped in MnO_2. The results obtained via the FTIR analysis confirm that Cu doped in MnO_2 nanoparticles was successfully developed. Thus, after doping with cu-ion the peaks at 3425 and 1647 cm^{-1} are stronger than those of the pure MnO_2, which indicates that cations dopant could facilitate the formation of hydroxyl OH^- or H_2O molecules.

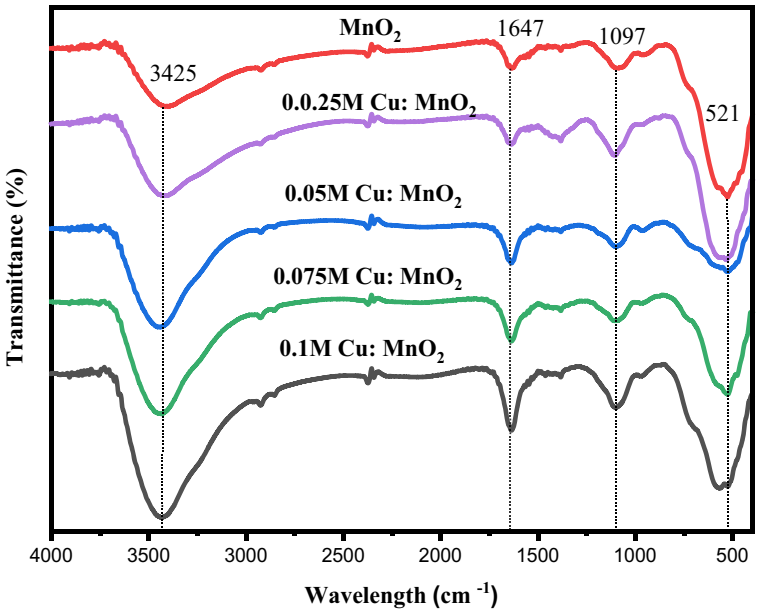

Fig. 3. FTIR spectra of pure MnO_2, and Cu doped α-MnO_2 nanoparticles.

3.3 Thermal Properties

To examine the thermal characteristics of MnO_2 and Cu doped MnO_2, TGA/DTA investigation have been examined in the temperature range of 30 °C–900 °C. The analysis was conducted with an increment of 10 °C per min in air atmosphere (Fig. 4). The TGA curve of MnO_2 displays three main weight losses in the temperature range of 30–129 °C, 130–534 °C, and 535–596 °C as shown in Fig. 4(a). The primary weight loss (0.38 mg) is associated with physically adsorbed water molecules, and the next (0.58 mg) corresponds with the phase change of MnO_2 to Mn_2O_3. Finally, the third phase of weight loss is associated with the phase change of Mn_2O_3 to Mn_3O_4. Hence, the analysis was started with 8 mg of MnO_2 and after exposed to 900 °C temperature, the remaining mass of MnO_2 was 6.85 mg with 14.38% weight loss. In the DTA analysis, the two endothermic and the exothermic peaks observed at 122 °C, 603 °C, and 807 °C indicates the elimination of physisorbed species, and the phase change from MnO_2 to Mn_2O_3 and Mn_3O_4, respectively. Similarly, The TGA curve of Cu doped MnO_2 exhibits three main weight losses in the temperature range of 30–315 °C, 316–534 °C, and 535–868 °C as shown in Fig. 4(b). The first weight loss (0.6 mg) ascribed to physisorbed species and the next (0.19 mg) is associated with the phase change of MnO_2 to Mn_2O_3. Finally, the third stage of weight loss (0.2 mg) is associated with the phase change of Mn_2O_3 to Mn_3O_4. Thus, the analysis was started with 8 mg of MnO_2 and after exposed to 900 °C temperature, the remaining mass of Cu doped MnO_2 was

7.01 mg with 12.34% weight loss. In the DTA analysis, the endothermic and the two exothermic peaks observed at 122 °C, 603 °C, and 807 °C indicates the elimination of physisorbed species, and the phase change from MnO_2 to Mn_2O_3 and Mn_3O_4, respectively. From the analysis Cu-doped MnO_2 nanoparticles showed good thermal stability with 12.34% weight loss.

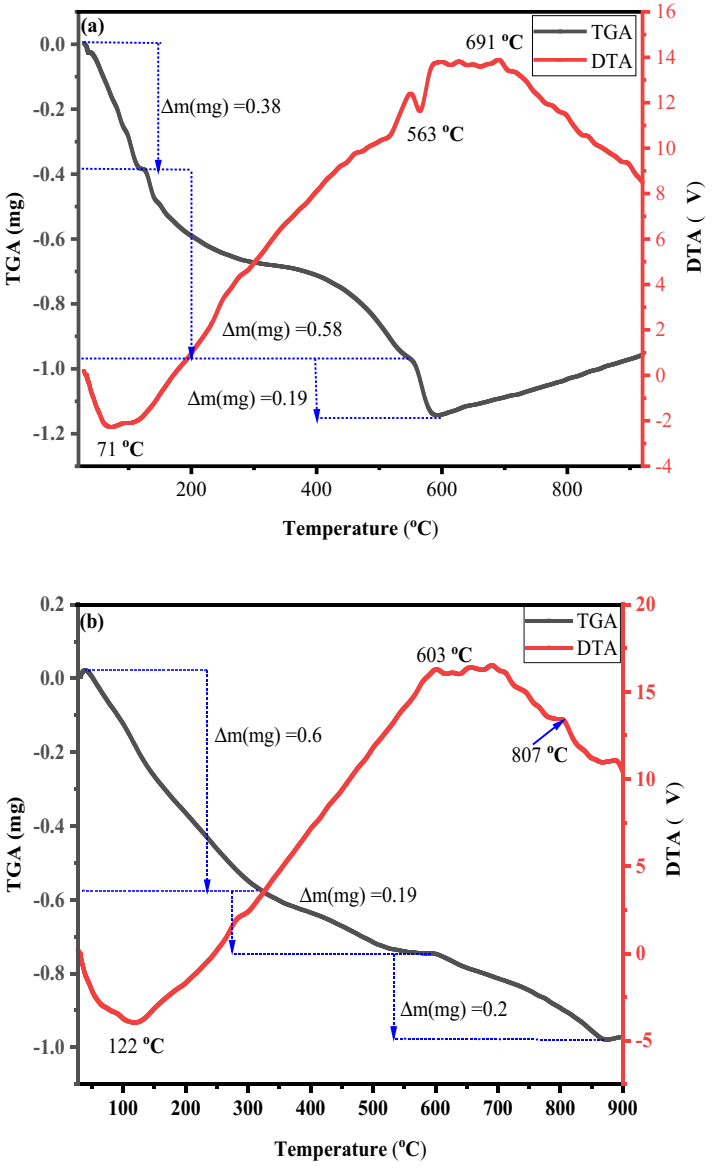

Fig. 4. TGA and DTA curve of (a) MnO_2 and (b) 0.1 M Cu doped α-MnO_2 nanoparticles.

3.4 Electrochemical Property Analysis

The ORR catalytic activity of the modified electrodes was investigated by CV in O_2 saturated in 0.1 M KOH aqueous solution at the scan rates of 50 mV s^{-1}, as shown in Fig. 5. The reduction peak was measured at −0.462V (vs. Ag/AgCl) for pure α-MnO_2.

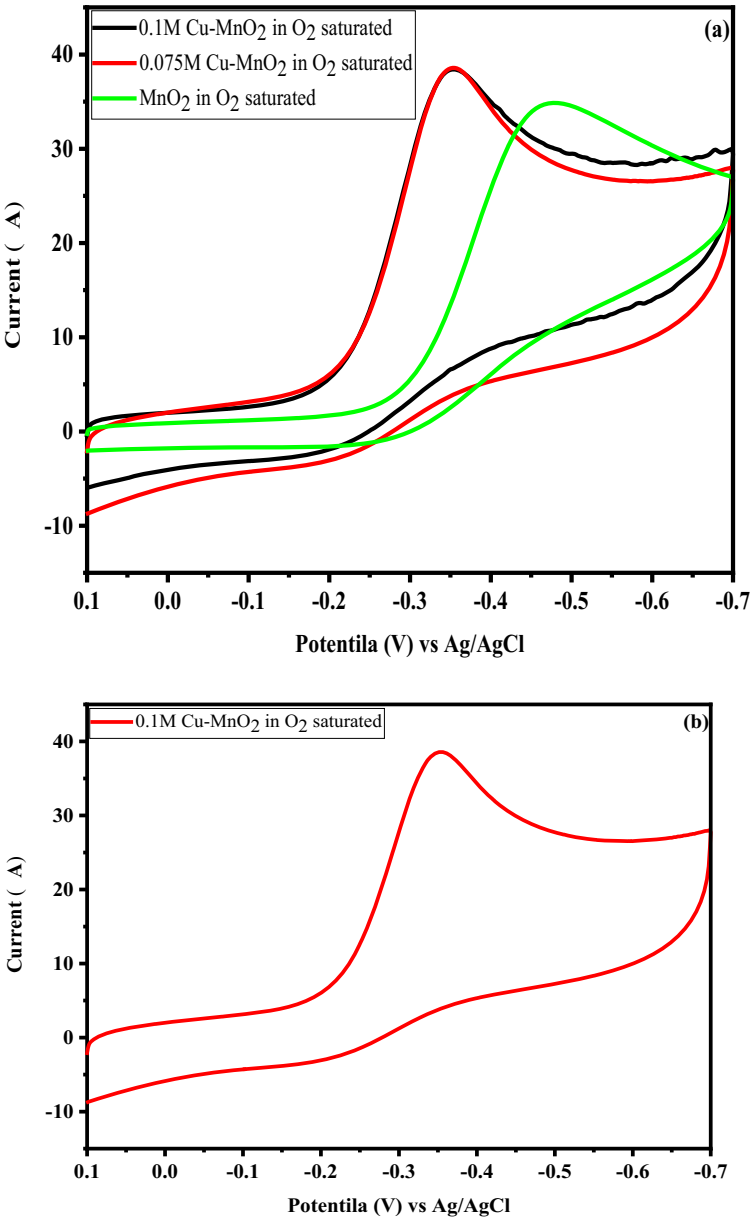

Fig. 5. CV curve of: (a) MnO_2 and Cu doped α-MnO_2 nanoparticles, (b) 0.1Cu doped MnO_2 of 20 cycles, at a scanning rate of 50 mVs^{-1}.

However, 0.075 and 0.1Cu doped MnO_2 showed enhanced reduction peak at −0.349 V (vs. Ag/AgCl) as shown in Fig. 5 (a). Hence, to determine the electrode stability of the Cu doped MnO_2 catalyst, a series of CV scans (of 20 cycles), at a scanning rate of 50 mVs^{-1}, for 0.1Cu doped MnO_2 nanoparticles was taken out as displayed in Fig. 5 (b). The result reveals that the positions of reduction peak of electrode did not exhibit any notable variation with the increasing cycles, showing excellent electrode stability [24]. Overall, the CV analysis confirmed that Cu doped α-MnO_2 is a promising ORR oxygen electrocatalyst.

4 Conclusions

In this paper, the structural, thermal and, electrochemical characteristics of MnO_2 and Cu-doped MnO_2 nanoparticles with different Cu concentrations synthesized by co-prescription technique have been studied. The XRD patterns showed that Cu ions substituted Mn ions without altering the tetragonal structure up to 0.1 M Cu-doping. However, the Crystallite size increases from 4.1 nm to 5.3 nm with an increment of dopant concentration to 0.1 M. TGA/DTA analysis confirmed that Cu doped MnO_2 nanoparticles show an improved thermal property. The catalytic characteristics of MnO_2 and Cu doped MnO_2 nanoparticles as an effective electrocatalyst for ORR in alkaline media were studied via CV. The catalytic activity of as-prepared catalysts was exactly connected with its crystal structure. The results gained in this study show that, the Cu doped MnO_2 nanoparticles possess higher catalytic activity than MnO_2 for ORR. Additionally, the CV measurements confirm that the dual impact within Cu and Mn improves the performance by breaking of O-O bond in oxygen. Hence, the excellent electrochemical properties of Cu doped MnO_2 nanoparticles for ORR addresses it as a promising candidate in different oxygen electrocatalytic utilization such as fuel cells and MABs.

Acknowledgements. This work was supported by Bahir Dar University, Bahir Technology of Institute, Bahir Dar Energy Center.

Conflicts of Interest. There is no conflict of interest concerning this article.

References

1. Poonguzhali, R., Shanmugam, N., Gobi, R., et al.: Effect of thermal annealing on the structural, morphological and super capacitor behavior of MnO2 nanocrystals. Mater. Sci. Semicond. Process. **27**, 553–561 (2014). https://doi.org/10.1016/j.mssp.2014.07.044
2. Zhu, J., Baig, S.A., Sheng, T., et al.: Fe3O4 and MnO2 assembled on honeycomb briquette cinders (HBC) for arsenic removal from aqueous solutions. J. Hazard. Mater. **286**, 220–228 (2015). https://doi.org/10.1016/j.jhazmat.2015.01.004
3. Lim, Y.G., Kim, H.J., Park, K.: A novel method for synthesizing manganese dioxide nanoparticles using diethylenetriamine pentaacetic acid as a metal ion chelator. J. Ind. Eng. Chem. **93** (2021). https://doi.org/10.1016/j.jiec.2020.10.019

4. Worku, A.K., Ayele, D.W., Habtu, N.G.: Recent advances and future perspectives in engineering of bifunctional electrocatalysts for rechargeable zinc–air batteries. Mater. Today Adv. **9**, 100116 (2021). https://doi.org/10.1016/j.mtadv.2020.100116
5. Baral, A., Satish, L., Padhy, S.K., et al.: Structure and activity of lysozyme on binding to lithium-manganese oxide nanocomposites prepared from seabed nodule. J. Phys. Chem. Solids **151** (2021).https://doi.org/10.1016/j.jpcs.2020.109794
6. Jõgi, I., Levoll, E., Raud, J.: Plasma oxidation of NO in O2:N2 mixtures: the importance of back-reaction. Chem. Eng. J. **301**, 149–157 (2016). https://doi.org/10.1016/j.cej.2016.04.057
7. Zhang, Y., Yue, D., Fang, D., et al.: Enhanced darkening effect from the interaction of MnO2 and oxygen on the component evolution of amino-phenolic humic-like substances. Chemosphere **263** (2021). https://doi.org/10.1016/j.chemosphere.2020.127956
8. Asiri, S.M.M., Cevik, E., Sabit, H., Bozkurt, A.: Alginate-guided size and morphology-controlled synthesis of MnO2 nanoflakes. Soft. Mater. **18** (2020). https://doi.org/10.1080/1539445X.2019.1672192
9. Cruz-Díaz, M.R., Arauz-Torres, Y., Caballero, F., et al.: Recovery of MnO2 from a spent alkaline battery leach solution via ozone treatment. J. Power Sources **274** (2015). https://doi.org/10.1016/j.jpowsour.2014.10.121
10. Ge, X., Liu, J., Song, X., et al.: Hierarchical iron containing γ-MnO2 hollow microspheres: a facile one-step synthesis and effective removal of As(III) via oxidation and adsorption. Chem. Eng. J. **301**, pp. 139–148 (2016). https://doi.org/10.1016/j.cej.2016.05.005
11. Wang, J., Tao, H., Lu, T., Wu, Y.: Adsorption enhanced the oxidase-mimicking catalytic activity of octahedral-shape Mn3O4 nanoparticles as a novel colorimetric chemosensor for ultrasensitive and selective detection of arsenic. J. Colloid Interface Sci. **584**, 114–124 (2021). https://doi.org/10.1016/j.jcis.2020.09.107
12. Ning, P., Lin, X., Wang, X., Cao, H.: High-efficient extraction of vanadium and its application in the utilization of the chromium-bearing vanadium slag. Chem. Eng. J. **301**, 132–138 (2016). https://doi.org/10.1016/j.cej.2016.03.066
13. Zhou, S., Shang, H., Luo, J., et al.: Organoarsenic conversion to As(III) in subcritical hydrothermal reaction of livestock manure. J. Hazard. Mater. **402** (2021). https://doi.org/10.1016/j.jhazmat.2020.123571
14. Maity, J.P., Chen, C.Y., Bhattacharya, P., et al.: Advanced application of nano-technological and biological processes as well as mitigation options for arsenic removal. J. Hazard. Mater. **405** (2021). https://doi.org/10.1016/j.jhazmat.2020.123885
15. Worku, A.K., Ayele, D.W., Habtu, N.G., et al.: Enhancing oxygen reduction reaction activity of ε-MnO2 nanoparticles via iron doping. J. Phys. Chem. Solids **157**, 110207 (2021). https://doi.org/10.1016/j.jpcs.2021.110207
16. Worku, A.K., Ayele, D.W., Habtu, N.G., et al.: Recent progress in MnO2-based oxygen electrocatalysts for rechargeable zinc-air batteries. Mater. Today Sustain. 100072 (2021). https://doi.org/10.1016/j.mtsust.2021.100072
17. Wu, K., Liu, T., Xue, W., Wang, X.: Arsenic(III) oxidation/adsorption behaviors on a new bimetal adsorbent of Mn-oxide-doped Al oxide. Chem. Eng. J. **192**, 343–349 (2012). https://doi.org/10.1016/j.cej.2012.03.058
18. Ding, B., Zheng, P., Ma, P., Lin, J.: Manganese oxide nanomaterials: synthesis, properties, and theranostic applications. Adv. Mater. **32**, 1905823 (2020). https://doi.org/10.1002/adma.201905823
19. Sun, H., Xu, K., Huang, M., et al.: One-pot synthesis of ultrathin manganese dioxide nanosheets and their efficient oxidative degradation of Rhodamine B. Appl. Surf. Sci. **357**, 69–73 (2015). https://doi.org/10.1016/j.apsusc.2015.08.258

20. Feng, L., Xuan, Z., Zhao, H., et al.: MnO2 prepared by hydrothermal method and electrochemical performance as anode for lithium-ion battery. Nanoscale Res. Lett. **9**, 290 (2014). https://doi.org/10.1186/1556-276X-9-290
21. Soejima, T., Nishizawa, K., Isoda, R.: Monodisperse manganese oxide nanoparticles: synthesis, characterization, and chemical reactivity. J. Colloid Interface Sci. **510**, 272–279 (2018). https://doi.org/10.1016/j.jcis.2017.09.082
22. Qin, M., Zhao, H., Yang, W., et al.: A facile one-pot synthesis of three-dimensional microflower birnessite (δ-MnO2) and its efficient oxidative degradation of rhodamine B. RSC Adv. **6**, 23905–23912 (2016). https://doi.org/10.1039/C5RA24848E
23. Chen, Y., Tian, Y., Qiu, Y., et al.: Synthesis and superior cathode performance of sandwiched LiMn2O4@rGO nanocomposites for lithium-ion batteries. Mater. Today Adv. **1**, 100001 (2019). https://doi.org/10.1016/j.mtadv.2018.12.001
24. Zhang, X., Yu, P., Zhang, D., et al.: Room temperature synthesis of Mn3O4 nanoparticles: characterization, electrochemical properties and hydrothermal transformation to $γ$-MnO2 nanorods. Mater. Lett. **92**, 401–404 (2013). https://doi.org/10.1016/j.matlet.2012.11.022